ELSEVIER

Palaeogeography, Palaeoclimatology, Palaeoecology 152 (1999) 283–303

PALAEO

Sedimentary cycles and volcanic ash beds in the Lower Pliocene lacustrine succession of Ptolemais (NW Greece): discrepancy between $^{40}Ar/^{39}Ar$ and astronomical ages

J. Steenbrink [a,*], N. van Vugt [b], F.J. Hilgen [a], J.R. Wijbrans [c], J.E. Meulenkamp [a]

[a] *Department of Geology, Faculty of Earth Sciences, Utrecht University, Utrecht, Netherlands*
[b] *Palaeomagnetic Laboratory 'Fort Hoofddijk', Faculty of Earth Sciences, Utrecht University, Utrecht, Netherlands*
[c] *Department of Geology, Faculty of Earth Sciences, Free University Amsterdam, Netherlands*

Received 23 February 1998; revised version received 19 November 1998; accepted 19 January 1999

Abstract

A high-resolution cyclostratigraphy for the rhythmically bedded lignite–marl sequences of the Lower Pliocene Ptolemais Formation is combined with $^{40}Ar/^{39}Ar$ dating results of intercalated volcanic ash beds. Detailed field reconnaissance in three open-pit lignite mines reveals three end-member sediment types: lignites, composed primarily of organic material; grey marls, a mixture of carbonate and organic material; and beige marls, almost exclusively composed of carbonate. These lithologies are arranged in two basic types of sedimentary cycles: lignite–grey marl and lignite–beige marl cycles. A cyclostratigraphic composite section comprising 56 lignite–marl cycles is constructed which combines the consistent cycle patterns from three parallel sections. The concordant positions of 20 volcanic ash beds in these sections confirm the cyclostratigraphic correlations and indicate that the lignite–marl cycles result from regional, basin-wide forcing rather than lateral facies migrations. $^{40}Ar/^{39}Ar$ ages on sanidine and biotite separates from nine volcanic ash beds were obtained by multiple total fusion and incremental-heating experiments. The $^{40}Ar/^{39}Ar$ ages range between 5.00 ± 0.05 and 4.04 ± 0.04 Ma and are, in general, consistent with the stratigraphic order. A least-square linear regression using the measured $^{40}Ar/^{39}Ar$ ages gives an average duration of 21.8 ± 0.8 kyr per lignite–marl cycle. Evidently, the lignite–marl cycles in the Ptolemais Formation are linked to the precessional variation in the Earth's orbit through its influence on Mediterranean climate. For the first time, $^{40}Ar/^{39}Ar$ dating results, totally independent from any other dating and or tuning technique, confirm the astronomical theory of climate change. The $^{40}Ar/^{39}Ar$ ages of the volcanic ash beds show a constant ~200 kyr (~4.5%) age discrepancy with the astronomical ages of the same ash beds. This inconsistency remains difficult to explain. The discrepancy is unlikely to have resulted from erroneous astronomical ages, through incorrectness in the astronomical tuning, inaccuracies of the magnetostratigraphic data or the orbital time-series used, and/or errors in the APTS. The $^{40}Ar/^{39}Ar$ dating results neither give clear indications for a possible source of error. From the excellent data set it is evident that neither loss of radiogenic ^{40}Ar, nor an underestimation of the contribution of Ca- and K-derived Ar isotopes could have caused the discrepancy. Moreover, the discrepancy is also beyond the errors in the systematic variables, like the decay constants of ^{40}K or the ages for the neutron-fluence monitors. © 1999 Elsevier Science B.V. All rights reserved.

Keywords: cyclostratigraphy; $^{40}Ar/^{39}Ar$ dating; lacustrine sediments; lignite; Pliocene; Greece

* Corresponding author. E-mail: jsteen@geo.uu.nl

0031-0182/99/$ – see front matter © 1999 Elsevier Science B.V. All rights reserved.
PII: S0031-0182(99)00044-9

1. Introduction

It has long been realised that marine sedimentary cycles may reflect climate oscillations that are controlled by the Earth's orbital cycles (Gilbert, 1895; Barrell, 1917). During the last decades, deep-sea oxygen isotope records fully confirmed that Pleistocene glacial cycles are driven by orbitally controlled variations in the solar radiation reaching the earth surface (Emiliani, 1955; Shackleton and Opdyke, 1973; Hays et al., 1976; Imbrie et al., 1984). More recently, the astronomical forcing and geochronological application of Milankovitch-type sedimentary cycles in deep-marine Pliocene and Miocene records in the Mediterranean Sea have been explored in detail (Hilgen, 1991; Krijgsman et al., 1995; Lourens et al., 1996). The tuning of such astronomically induced sedimentary sequences to computed time series of past variations in the Earth's orbit (or to derived target curves, e.g. insolation or ice sheet volume) has led to the construction of an astronomically calibrated polarity time scale (APTS) for the marine record which has been extended back to 12 million years (Hilgen et al., 1995; Krijgsman et al., 1995; Shackleton et al., 1995).

Orbital influences are not restricted to open marine systems, but are found in all types of sedimentary environments, including lacustrine successions (Bradley, 1929; Van Houten, 1964; Fischer, 1980; Anderson, 1982). Ideally, sections with a continuous cyclic pattern and good time control are used in studying the role of orbital forcing. Cyclostratigraphic studies on lacustrine sediments are hampered by a large degree of lateral variability, the scarcity of long continuous outcrops and the general lack of direct and precise time control. Yet, the complete and almost undisturbed lacustrine sequences of the Lower Pliocene Ptolemais Formation in the intermontane Ptolemais Basin (NW Greece) are an exception. These successions are excellently exposed in open-pit lignite mines and show an often prominent alternation of lignite–marl cycles. Intercalated volcanic ash beds throughout the entire Ptolemais Formation serve as important time marker horizons for stratigraphic correlations. $^{40}Ar/^{39}Ar$ dating of these volcanic ash beds provides significant time calibration points for the record and concomitant magnetostratigraphic studies (Van Vugt et al., 1998) give accurate time control as well.

In this paper, the cyclostratigraphic properties of the Ptolemais Formation will be discussed along with $^{40}Ar/^{39}Ar$ dating results on nine intercalated volcanic ash beds. The $^{40}Ar/^{39}Ar$ ages will be compared with astronomical ages for the same volcanic ash beds. The former ages are based on the radioactive decay of ^{40}K. The latter ages were independently obtained by magnetostratigraphic calibration to the APTS and subsequent correlation of the sedimentary cycles to computed astronomical target curves by Van Vugt et al. (1998). Their palaeomagnetic data, combined with the cyclostratigraphic framework and $^{40}Ar/^{39}Ar$ dating results presented in this paper, provide the necessary high-resolution time frame for further palaeoclimate and palaeoenvironment studies on the Ptolemais area.

2. Geological setting and stratigraphy

The elongated intermontane Ptolemais Basin is part of a NNW–SSE trending graben system that extends over a distance of 250 km from Bitola in the Former Yugoslavian Republic of Macedonia (F.Y.R.O.M.) to the village of Servia, southeast of Ptolemais, Greece (Fig. 1). The depression is filled with a 500–600 m thick succession of Upper Miocene to Lower Pleistocene, predominantly lacustrine sediments with intercalated lignite seams and fluvial deposits, schematically indicated in Fig. 1.

The basin is bounded by two fault systems, which can be related to two extensional episodes (Pavlides and Mountrakis, 1986; Mercier et al., 1989). The first, Late Miocene episode resulted in the origin of the basin in response to NE–SW extension. The second, Pleistocene episode of NW–SE extension resulted in the development of a sequence of subbasins. Currently, the basin is situated about 700 m above sea level. The depression is surrounded by the mountain-ranges of Vermio (2052 m) to the east and Askio (2111 m) to the west, which are mainly composed of Palaeozoic schists and Mesozoic limestones (Brunn, 1956; Kaouras, 1989) (Fig. 1).

Following previous investigations (Ehlers, 1960; Anastopoulos and Koukouzas, 1972), three basin-wide lithostratigraphic units can be recognised in

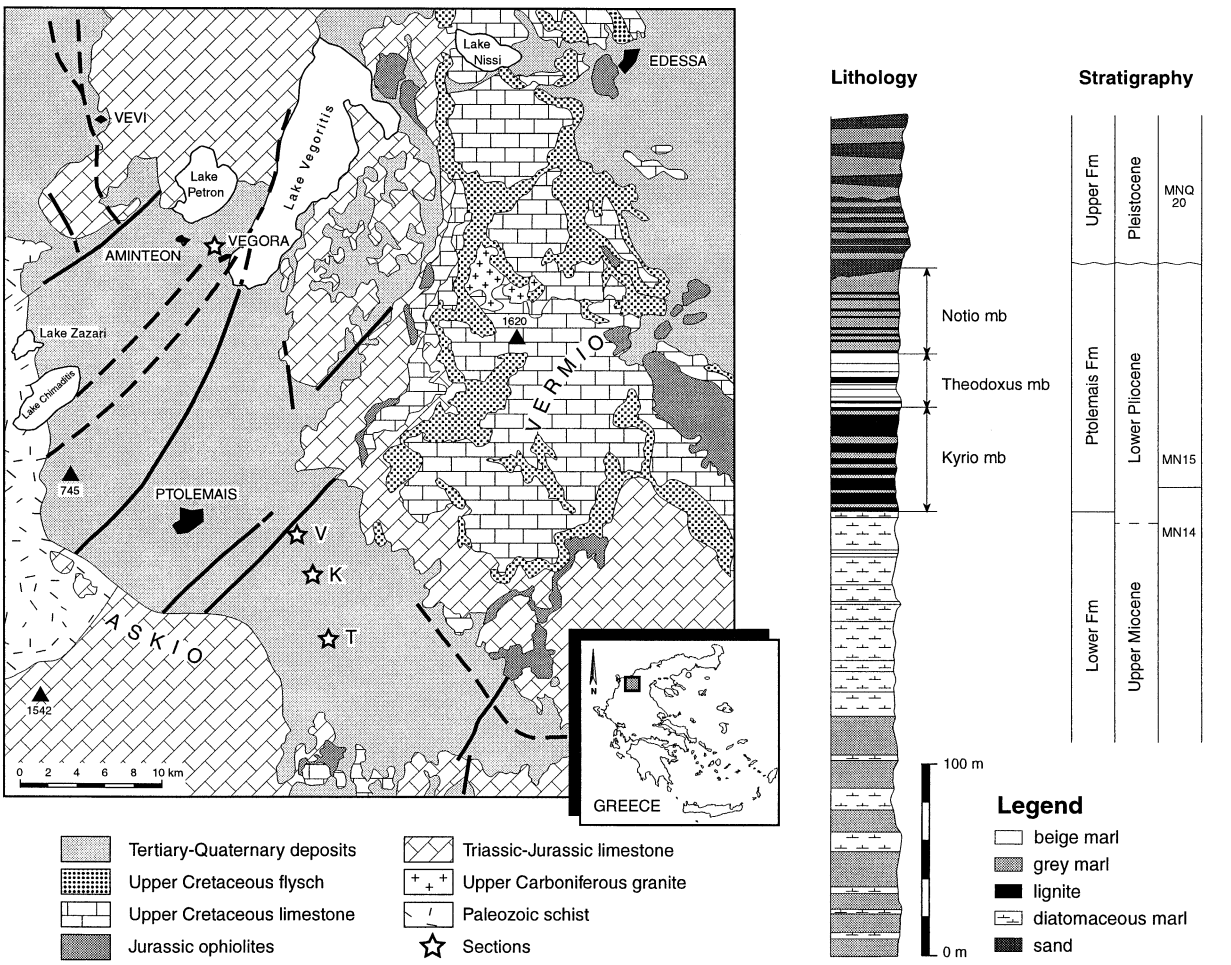

Fig. 1. (Left) Simplified geological map of the Ptolemais Basin in NW Greece showing the location of the Vorio (*V*), Komanos (*K*) and Tomea Eksi (*T*) sections (modified after Papakonstantinou, 1979). (Right) Generalised stratigraphy of the Neogene sedimentary sequence in the Ptolemais area. Lithology slightly modified after Anastopoulos and Koukouzas (1972); Formations and members after Ehlers (1960); *MN* and *MNQ* (micro-mammal) zones from Van de Weerd (1979) and Koufos and Pavlides (1988).

stratigraphic order: the Lower Formation, the Ptolemais Formation and the Upper Formation (Fig. 1). The Lower Formation is approximately 300 m thick and unconformably overlies the pre-Neogene basement. Information is mainly derived from drillings. It is predominantly composed of lacustrine (sometimes diatomaceous) marls with some prominent intercalated lignite seams. Plant remains from the middle part of the Lower Formation point to a Late Miocene age (Gregor and Velitzelos, 1995).

The next higher Ptolemais Formation, with a thickness of approximately 110 m, has been subdivided into the Kyrio, Theodoxus and Notio members (Fig. 1). The lowermost Kyrio member consists of rhythmic alternations of lignite and grey marl beds (Fig. 2A). These alternations pass laterally into a succession predominantly composed of lignite with only minor intercalations of marls and/or sand lenses. The base of the Kyrio member reflects the onset of Pliocene lignite accumulation in the Ptolemais Basin. The first abundant occurrence of the characteristic freshwater gastropod *Theodoxus macedonicus* defines the base of the next-higher unit. The middle Theodoxus member includes two pre-

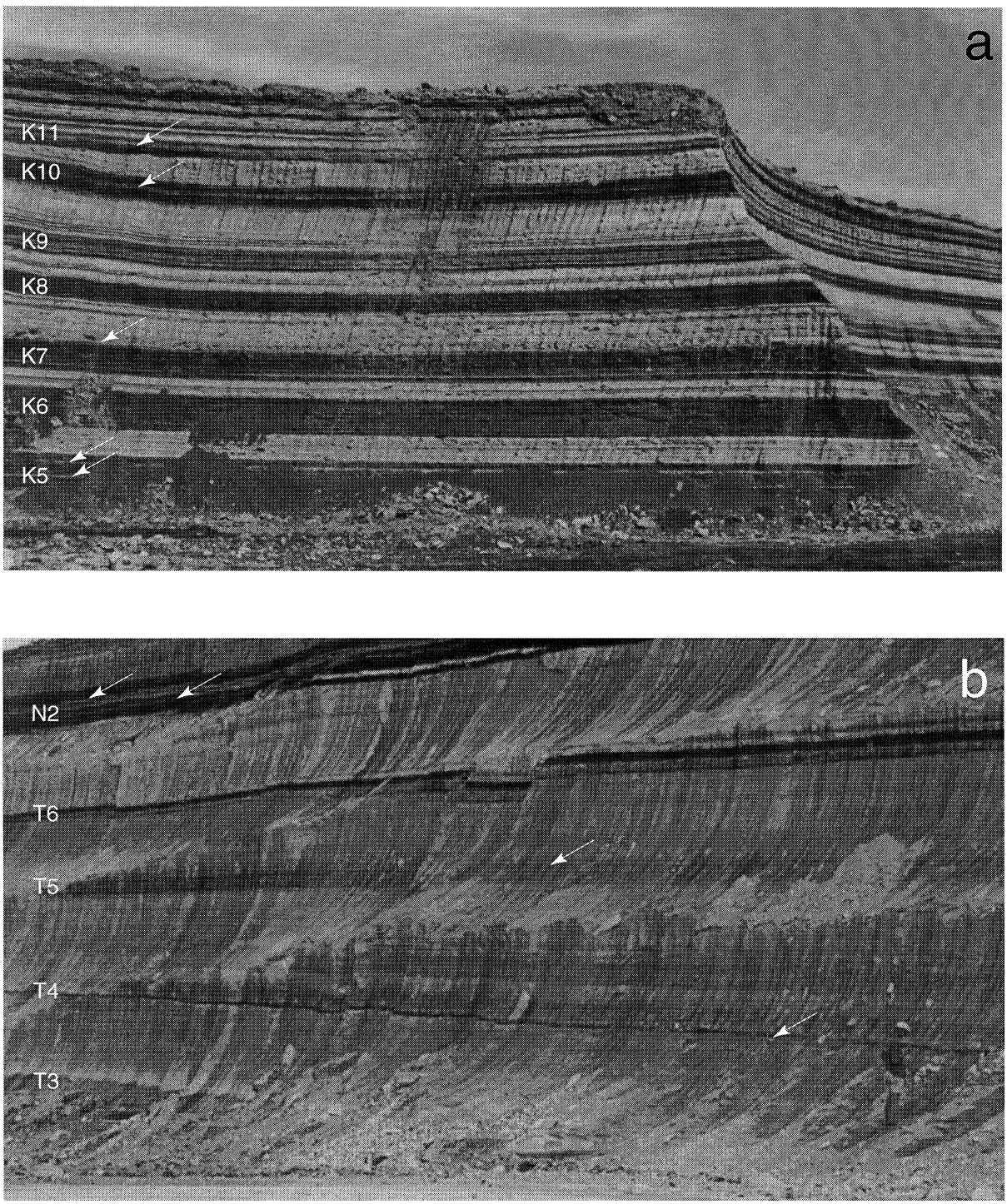

Fig. 2. (A) Komanos open-pit mine. Lignite–grey marl cycles K5 to K11 of the Kyrio member. Arrows denote positions of the volcanic ash beds in cycles K5, K7 (the so-called layer 9; Van de Weerd, 1983), K10 and K11. (B) Vorio open-pit mine. Lignite–beige marl cycles T3 to T6 of the Theodoxus member, and lignite–grey marl cycles N1 (poorly developed) and N2 from the Notio member. Arrows denote positions of the volcanic ash beds in cycles T4, T5 and N2.

Fig. 2 (continued). (C) Tomea Eksi open-pit mine. Lignite–beige marl cycles T5 and T6 of the Theodoxus member, and lignite–grey marl cycles N1 to N4 of the Notio member. Arrows denote positions of the volcanic ash beds in cycles T5, N2 and N3.

dominantly beige-coloured marl intervals, separated by a prominent lignite bed (Fig. 2B). The distinctive change in colour from beige to grey marls marks the transition towards the next-higher unit. This uppermost unit, the Notio member, is composed of lignite–grey marl rhythmites (Fig. 2C). In the upper part of this unit, the lignite–grey marl rhythmites pass laterally into banded xylite. Pollen, mollusc and micro-mammal studies indicate an Early Pliocene age for the Ptolemais Formation (Vetoulis, 1957; Gramann, 1960; Van de Weerd, 1979).

The Upper Formation unconformably overlies the Ptolemais Formation; it consists of up to 200 m of fluvio-lacustrine marls with intercalated clay, sand and conglomerate beds (Fig. 1). The succession includes a vertebrate fauna of Pleistocene age (Velitzelos and Schneider, 1973; Koufos and Pavlides, 1988).

In this contribution, we will only consider the cyclostratigraphy and $^{40}Ar/^{39}Ar$ dating results for the Ptolemais Formation. In a forthcoming paper, we will discuss the stratigraphic framework for the Lower Formation.

3. Sediment types and cyclostratigraphy

Ideally, continuous cyclic successions are used in studying the role of orbital forcing. Such ideal conditions do not exist everywhere in the Ptolemais record. The sediments show a considerable degree of lateral variability. Moreover, in some parts of the sequence, the occurrence of fossiliferous lenses and discontinuous channel fills may reflect periods of erosion and non-deposition. Both the lateral variability and local presence of minor gaps in the sedimentary record hamper a straightforward interpretation of the succession in terms of sedimentary cycles.

Detailed field reconnaissance in three open-pit lignite mines (Fig. 1) reveals that the successions in each open-pit contain both intervals in which the cyclic alternations of lignites and marls is very prominent, and intervals where indications for cyclic sedimentation are less obvious or even absent. We logged representative sections in the three open-pits, focusing on the rhythmic lignite–marl patterns. Through careful comparison of outcrops all over the mining area, local features could be separated from

consistent (i.e. laterally continuous) patterns. The results will be discussed below. Firstly, the sedimentological characteristics of the three main sediment types constituting the rhythmic alternations — lignite, grey marl and beige marl — will be considered. Secondly, the two basic types of sedimentary cycles, i.e. lignite–grey marl and lignite–beige marl cycles, will be dealt with. Finally, the cyclic patterns of alternating lignite and marl beds are discussed for each stratigraphic unit, thus providing the basis for a cyclostratigraphic composite section showing an 'ideal' succession of cycles for the Ptolemais Basin.

3.1. End-member sediment types

The Ptolemais Formation contains two major sediment types: dark-coloured lignites and light-coloured marls. Considering colour, composition and fossil content, grey and beige marls can further be distinguished. For this study, the terminology of Bates and Jackson (1987) is used, defining marl as a soft, earthy material, largely composed of carbonate precipitated in freshwater lakes and ponds. The three sediment types — lignite, grey marl and beige marl — are so-called end-members, i.e. they form the primary components of a variety of lithologies. One of the general characteristics of the three sediment types is the low concentration of non-combustible material such as terrigenous clastics or siliceous microfossils (diatoms). In contrast, organic and carbonate components together constitute generally more than 95% by weight. Of primary interest in this study are the rhythmic alternations of lignite and marl beds in the Ptolemais Formation. Therefore, only the sedimentological properties of these sediment types will be discussed in the following section.

Lignites. The lignites of the Ptolemais Formation are primarily composed of fine-grained organic material. Larger fragments of fossil plant tissue (mainly reed and root remains) are common, wood remains are rare. Both massive lignites without macroscopic structure and finely bedded lignites occur. The lignite beds contain fossiliferous levels mostly in lags with small mammal associations, fish remains, freshwater pelecypods and gastropods. The total organic matter content is around 90%. As a rule individual lignite beds of lignite–marl cycles are some dm to 2 m thick (Fig. 2A,C and Fig. 3). Thin (cm-scale) lignite layers are present within most marl beds.

The extensive character of the lignite beds, their composition as well as the faunal content of the associated strata suggest formation in a reed swamp environment. Van de Weerd (1983) came to the same interpretation based on palynological studies. This is in accordance with the classification of the lignites as huminite-rich brown coals by Cameron et al. (1984) and Kaouras (1989).

Grey marls. The grey marls represent a mixture of predominantly homogeneous carbonate and organic plant debris. Bioturbation, chiefly by roots, is pervasive. The rich biota is dominated by shallow-water lacustrine gastropods (e.g. *Planorbis planorbis*, *Valvata cristata* and *Lymnea stagnalis*) and ostracods, and furthermore characterised by the near-absence of aquatic macrophytes. Seeds of typical reed plants are abundant. The samples contain up to 30% of organic matter and between 70 and 95% of carbonate by weight. Individual grey marl beds, often with thin lignite interbeds, are up to 2 m thick, and can generally be traced from one section to another. Such beds are only found in the Kyrio and Notio members (Fig. 2A,C and Fig. 3).

The lateral extent, composition and gastropod assemblages of the grey marl beds point to deposition in a flat marginal, shallow lacustrine environment with abundant plant growth. This is also indicated by the intense bioturbation and general absence of aquatic macrophytes, which prefer more open lacustrine conditions (Dean and Fouch, 1983).

Beige marls. The beige marls contain as much as 95% carbonate and only a few percent of organic matter. Calcite is the predominant carbonate min-

Fig. 3. Lithostratigraphy and cyclostratigraphy of the Vorio, Komanos and Tomea Eksi sections. In the lithological column, black (grey) indented beds denote lignite (marly equivalent of lignite) beds, grey (white) protruding beds denote grey (beige) marl beds, thin extra protruding layers denote volcanic ash beds and dark grey indented layers in the basal part of Vorio denote sand lenses. Dashed lines correlate individual ash beds. The sedimentary cycles have been numbered from base to top for each member where *K* refers to the Kyrio member (cycles K1–K30), *T* to the Theodoxus member (cycles T1–T6) and *N* to the Notio member (cycles N1–N20).

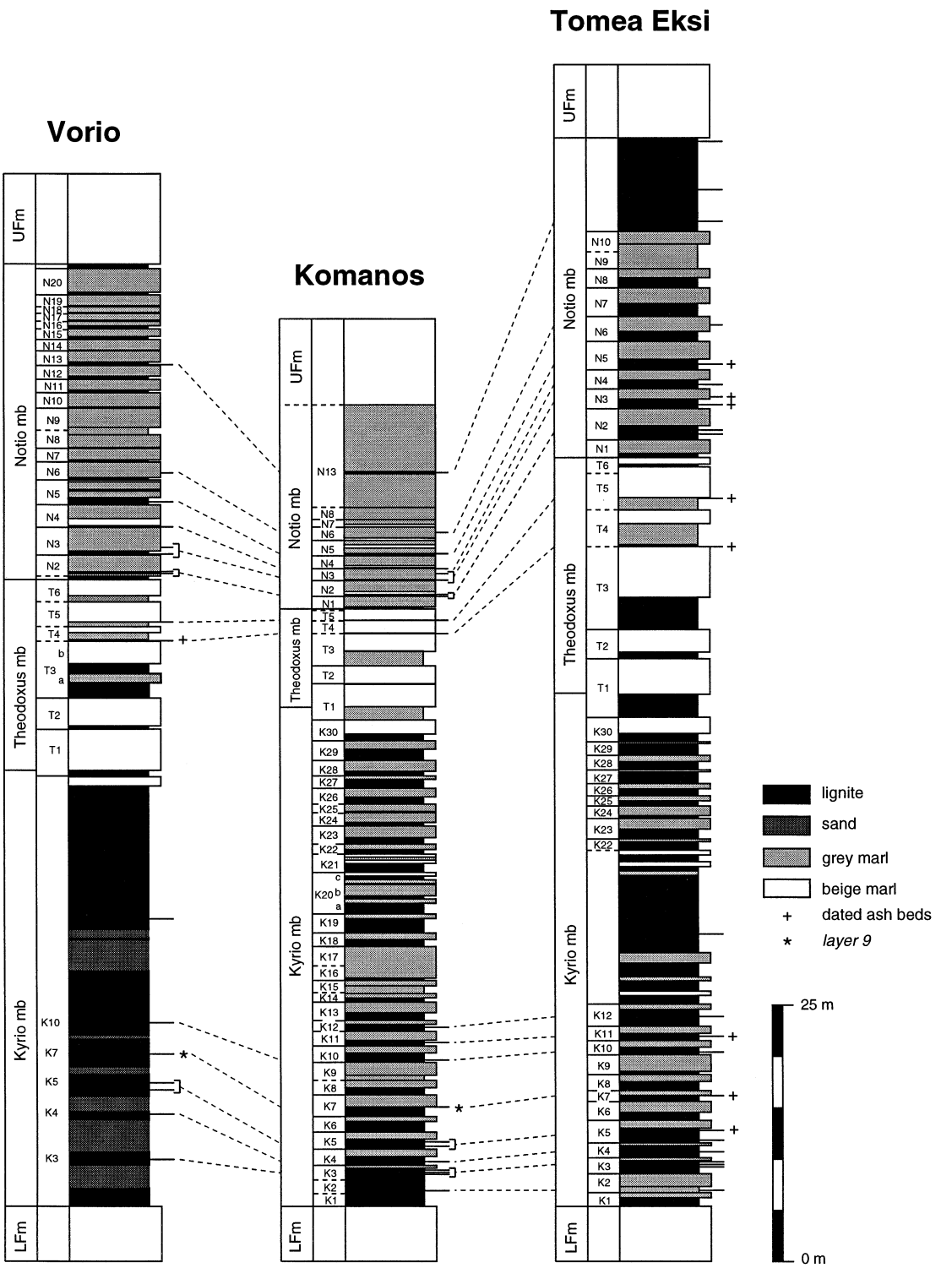
Vorio
Komanos
Tomea Eksi
UFm
Notio mb
Theodoxus mb
Kyrio mb
LFm
lignite
sand
grey marl
beige marl
+ dated ash beds
* layer 9
25 m
0 m

eral. The organic fraction is dominated by aquatic plant fragments. The biota is dominated by lacustrine bottom-dwelling gastropods (e.g. *Theodoxus macedonicus* and *Valvata hellenica*) and stem encrustations of the chlorophyte *Chara*. Root imprints are generally absent. Individual beige marl beds have a thickness between 0.2 and 2 m, showing large lateral thickness variations both within and between the open-pit mines studied. The beige marl beds are mainly found in the Theodoxus member (Fig. 2B and Fig. 3).

The gastropods *Theodoxus macedonicus* and *Valvata hellenica* prefer open lacustrine conditions devoid of bottom vegetation (Gramann, 1960). The chlorophyte *Chara* thrives in littoral lacustrine conditions, with a lower limit of deposition normally between 4 and 6 m below lake level (Dean and Fouch, 1983). The absence of lamination suggests shallow, oxygenated conditions. Comparison with recent analogues (Murphy and Wilkinson, 1980) leads us to suggest that the Ptolemais beige marls were deposited on the marl bench platform and/or slope. The observed large lateral variability of individual beige marl beds is consistent with this interpretation.

3.2. Basic types of sedimentary cycles

The occurrence on various scales of alternating dark-coloured lignites and light-coloured marl beds is the most obvious characteristic of the Ptolemais Formation (Figs. 2 and 3). These sedimentary colour couplets represent rhythmic lignite and marl alternations. On a metre scale two basic types of sedimentary cycles can be distinguished: lignite–grey marl and lignite–beige marl cycles.

Lignite–grey marl cycles. The bipartite lignite–grey marl cycles display black–grey colour alternations. This type of cycle ranges in thickness from 1.1 to 2.5 m and consists of some dm to 2 m of black-coloured lignite at the base followed by a grey marl bed, usually with cm-thick lignite interbeds (Fig. 2A,C). Lignite–grey marl cycles are clearly developed in the Kyrio and Notio members (Fig. 3). The lignite and marl segments of individual cycles display considerable lateral variations in thickness. For instance, the cycles in the Notio member of the Tomea Eksi section have considerably thicker lignite beds than those in the Vorio section (Fig. 3). The grey marl segments of the same cycles show an opposite trend, that is, thicker in the Vorio section with respect to the Tomea Eksi section.

Lignite–beige marl cycles. Individual bipartite lignite–beige marl cycles display black or brown and beige colour alternations and range in thickness from 1.0 to 5.5 m. Such cycles are most pronounced in the Theodoxus member and consist of a basal black lignite or dark-coloured marl bed topped by a beige marl bed (Fig. 2B and Fig. 3). The beige marl beds display a subtle colour banding. The lignite–beige marl cycles show considerable lateral variation between the sections, both in cycle-thickness and in thickness of individual lignite and beige marl beds (Fig. 3).

3.3. Cyclostratigraphic framework

Evidently the cyclicity is not uniform throughout the entire sequence; specific intervals show quite regular lignite–marl cycles, whereas others are composed of less well developed cycles. In addition, the type of cyclicity, i.e. lignite–grey marl or lignite–beige marl is confined to specific intervals. The cyclostratigraphic details will be presented below in stratigraphic order for each member, where ‘K’ refers to Kyrio, ‘T’ to Theodoxus and ‘N’ to Notio. The sedimentary cycles have been numbered from base to top for each member: K1–K30 for the Kyrio member, T1–T6 for the Theodoxus member and N1–N20 for the Notio member (Figs. 2 and 3).

3.3.1. Kyrio member

Considering the expression and lateral consistency of the alternating lignite and marl beds, the Kyrio member was subdivided into three stratigraphic intervals. The lower interval, spanning cycles K1 to K12, consists of clear lignite and marl alternations in at least one section. The same holds for the upper interval, cycles K23 to K30. The sedimentary expression of lignite and marl alternations in the middle interval, which contains cycles K13 to K22, is less pronounced in the studied sections.

Cycles K1 to K12. These cycles are apparent as rhythmic alternations of lignite and grey marl beds in the Tomea Eksi section (Fig. 3). In the Komanos section, cycles K4 to K12 show essentially the same cyclic lignite–grey marl alternations (Fig. 2A and

Fig. 3). The occurrence and number of volcanic ash layers in both sections in the cycles K2, K3 (three ash beds), K4, K5 (two ash beds), K7, K10, K11 and K12 confirm the cyclostratigraphic correlations, and show that the rhythmic alternations are synchronous. Additional evidence for the proposed correlation between the two sections is provided by cycle K9, which has a poorly developed basal lignite bed in contrast to the other cycles in this part of the sequence. The general lack of grey marl beds in the Vorio section impedes the recognition of individual cycles. However, the unusually thick volcanic ash layer in cycle K7 — the so-called layer 9 (Van de Weerd, 1983) — as well as the consistent presence of additional, particular, mm-thick volcanic ash beds below and above this ash bed, enable a detailed correlation with the corresponding interval of the pronounced cyclically bedded Komanos and Tomea Eksi sections.

Cycles K13 to K22. The cyclostratigraphic interpretation of this interval is not very straightforward. Only the Komanos section comprises alternating lignite and grey marl beds. In the Vorio and Tomea Eksi sections the corresponding interval consists of an extensive, thick lignite seam with only a few, subordinate marl intercalations; abundant fossiliferous lenses suggest episodes of erosion and/or non-deposition. Even in the Komanos section, the expression of the sedimentary cyclicity is not very distinct. The basal lignite layers of cycles K15, K17 and K18 alternate with thin grey marl beds. This holds in particular for cycle K17, which contains alternating thin lignite and marl layers extending from marl K16 to lignite K18. The thickness of the combined marl bed of K16–K17 led to the interpretation of K17 as a separate cycle. The interval between K19 and K21 lacks a clear cyclicity. It contains a distinct basal lignite bed, followed by alternating lignite, grey and beige marl beds. The banded interval is approximately three times thicker than the average cycle thickness. Therefore, it might represent three cycles (K20a, b, and c), but the lack of distinct lignite layers hampers an unambiguous cycle definition for this interval.

Cycles K23 to K30. These cycles in Komanos and Tomea Eksi are apparent as rhythmic alternations of lignite and grey marl beds. The expression of the cyclicity is clearer in Tomea Eksi due to the presence of more prominent basal lignite beds as compared to Komanos. Notable is the fact that the marl segments of cycles K27 and K29 in Tomea Eksi are very thin or sometimes even absent in contrast to the other cycles which have a ‘normal’ marl segment. In Komanos the marl segments of cycles K25 and K27 are thinner than average. Cycle K30 comprises a pronounced beige marl bed. The general lack of marl beds in the Vorio section prevents a clear recognition of sedimentary cycles in the corresponding interval of cycles K23 to K30.

3.3.2. Theodoxus member

The Theodoxus member consists of two beige marl beds with thin lignite intercalations, separated by a prominent lignite bed. The lower marl bed is separated in two by a thin lignite bed and therefore interpreted to comprise two lignite–beige marl cycles, T1 and T2 (Fig. 3). The upper part of the Theodoxus member includes a banded beige marl bed with some two to four thin lignite seams. However, the lack of distinct lignite beds and the great lateral changes in bed-thickness hinder an unambiguous cyclostratigraphic interpretation for this interval. In the Vorio section, the expression of the cyclicity is most clear, showing three light–dark alternations (Fig. 2B). Therefore, this upper beige marl interval is interpreted to portray cycles T4, T5 and T6 (Fig. 3). The prominent lignite bed in Vorio separating the lower and upper beige marl bed contains a grey marl bed, which might suggest that it includes an extra cycle. Therefore, cycle T3 is numbered as T3a and T3b (Fig. 3). The volcanic ash beds in cycles T4 and T5 confirm our cyclostratigraphic correlations, showing that these lignite–marl cycles in the different sections are synchronous.

3.3.3. Notio member

In view of the expression and lateral continuity of the lignite and marl alternations, the Notio member was subdivided into two parts. The lower interval, spanning cycles N1 to N10, consists of clear lignite and marl alternations in all three sections. Alternating lignite and marl beds in the upper interval, spanning cycles N11 to N22, are only found in the Vorio section.

Cycles N1 to N10. In all three studied sections, this interval displays a clear rhythmic alternation of

lignite and primarily grey marl beds (Fig. 3). Ten complete lignite–grey marl cycles are recorded in the Tomea Eksi and Komanos sections. In the Vorio section, the first cycle (N1) is poorly developed or missing. In Vorio and Komanos, the basal lignite beds are generally thinner than in Tomea Eksi. Consequently, the cyclicity is more distinct in the latter section. Again, the occurrence, position and number of volcanic ash layers in cycles N2 (two ash beds), N3 (two ash beds), N4, N5 and N6 confirm our correlations between the different sections, and show that the lignite–marl cycles are time-equivalent. Additional evidence is provided by the relatively thick grey marl bed of cycle N5 and the lack of a distinct basal lignite bed in cycles N9 and N10.

Cycles N11 to N20. In the Vorio section, ten additional lignite–grey marl cycles have been recorded. In these cycles, grey marl beds alternate with thin lignite beds. Some characteristic cycle patterns can be distinguished in addition to the basic cycle repetition. Cycles with distinct lignite (N11 to N13, and N16) alternate with cycles in which lignites are weakly developed (N14, N15, and N17 to N19). In the Tomea Eksi section, lignite predominates above cycle N10, whereas in the Komanos section grey marl predominates, which in both cases impedes a further recognition of sedimentary cycles for this interval.

4. Argon geochronology

We performed both incremental-heating and laser total fusion $^{40}Ar/^{39}Ar$ dating on the Ptolemais volcanic ashes complementing our cyclostratigraphic study. Nine ash beds were analysed, three from each stratigraphic member (Fig. 3). Isotopic dating focused on the sanidine populations of these ash beds, because of the generally good preservation and high K-content of the individual crystals. In general, the biotite crystals have been partially altered to chlorite and are therefore less suitable for dating. The only exception is the ash bed in cycle T5 in the Theodoxus member, which contains fresh and unaltered biotite crystals. Because of their continuity and uniform thickness, the ash beds are interpreted as primary fall-outs, with only limited post-depositional transport. All but one appear as a few-mm to three-cm thick partings. Ash bed K7 — the so-called layer 9 (Van de Weerd, 1983) — about 10 m above the base of the Ptolemais Formation, has a thickness of about 25 cm. Explosive acid volcanic activity is common in the area from Miocene to Recent, and thought to be related to subduction related magmatism (Kolios et al., 1980).

4.1. Methods

Bulk samples with a weight of ca. 1 kg were washed and sieved to separate the >125 μm fraction. An optimum sieve fraction between 125 μm and 500 μm was selected for further separation. Mineral separates of sanidine and biotite were concentrated by standard heavy liquid and magnetic separation techniques, and finally by hand-picking the clear (fresh) phenocrysts under a binocular microscope. Sample purity and mineralogy of the sanidine separates was assessed by non-destructive X-ray fluorescence (XRF) analyses on the actual separates. The K/Ca ratios for all separates were ~10, which is indicative for the K-feldspar sanidine.

$^{40}Ar/^{39}Ar$ analyses were performed in 1996 and 1997 (irradiation runs VU16 and VU21) on the argon laser-probe facility (VULKAAN) at the Free University in Amsterdam, the Netherlands. A detailed description of the techniques is given by Wijbrans et al. (1995). Approximately 50-mg aliquots of the purified mineral separates were wrapped in Al foil and loaded in 5 mm ID quartz reactor vials. Irradiation with fast neutrons was done in the Oregon State University TRIGA reactor in the cadmium shielded CLICIT facility for 2 h (VU16) and 7 h (VU21). To monitor the variation in neutron flux over the entire length of the irradiation vials, neutron-fluence monitors were loaded at the top and bottom positions of the tube and between each set of four or five unknowns. The monitor mineral used in VU16 was sanidine DRA from the trachite from Drachenfels, Germany (Wijbrans et al., 1995). The age used for this standard has been determined by intercalibration against Taylor Creek Rhyolite sanidine (sample TCR 85G003 of Dalrymple and Duffield, 1988). The error-weighted mean age of 48 analyses vs. an age of 27.92 Ma for TCR was 24.99 ± 0.14 Ma for DRA (Wijbrans et al., 1995). The age of TCR is relative to a K–Ar age of 162.9 Ma of the primary stan-

dard SB-3 biotite (Lanphere et al., 1990). VU21 was monitored with DRA, TCR and FCT sanidines. An internally consistent J-curve was calculated from multiple analyses, using and age of 27.92 Ma for TCR, 24.99 Ma for DRA and 27.62 Ma for FCT. The age of 27.62 Ma for FCT is based on unpublished, internal calibrations of multiple irradiation runs with TCR and DRA.

Subsequent to irradiation, the samples were transferred into 2 mm diameter wells in a copper sample holder for laser fusion, placed in an ultra-high-vacuum extraction line and preheated to 200ºC for 24 h in order to remove undesirable large quantities of atmospheric argon from the line. The samples were fused using a focused continuous ion laser beam (max. 18 W), applied for 60 to 90 s. After an additional 5-min of clean-up, the isotopes of the purified argon gas were measured using a Mass Analyser Products LTD 215-50 noble gas mass spectrometer. Beam intensities were measured in peak jumping mode over the mass range 40–36 on a secondary electron multiplier and regressed to the height at the time of the inlet. The laser incremental-heating experiments consisted of 8 to 14 individual steps, degassing approximately 50 grains. We defocused the laser beam and increased the power of the laser for each subsequent step. In the laser total fusion experiments, five separate splits of approximately 25 grains were analysed. Here, we used a focused laser beam.

Each analysis was corrected for mass discrimination and a total system blank at the five Ar mass positions. System blanks were measured between every five steps. Mass discrimination during this study as monitored by aliquots of air from an on-line air pipette system was 1.0029 per mass unit for VU16 and 1.0038 for VU21. The total system blanks for this project were in the range 1.1 to 6.0×10^{-17} moles for $m/e = 40$, 0.4 to 4.3×10^{-19} moles for $m/e = 39$, 1.1 to 5.3×10^{-19} moles for $m/e = 38$, 1.7 to 2.5×10^{-18} moles for $m/e = 37$ and 3.3 to 7.9×10^{-19} moles for $m/e = 36$. The neutron-fluence parameter J was calculated from five to twelve replicate total fusion analyses of 10 to 15 grains of the monitor standards. J for each point in the quartz tube was determined using a second-order polynomial regression between individual standards, what resulted in best-fit curves with R^2 of 0.98 (VU16) and 0.93 (VU21). Reproducibility of each monitor point along the J curve suggests that errors in the J value are around 0.3%; this error was propagated into the age calculations for each analysis. MSWD calculations were also made to test for scatter about the mean. Ages were calculated using the decay constants of Steiger and Jaeger (1977). All the error assignments throughout this paper are $\pm 2\sigma$.

4.2. Results

The results from the incremental-heating experiments are presented in age spectrum diagrams (Fig. 4). Age plateaux are reported in this study, because the uniformly high radiogenic Ar yields of individual gas fractions (90–99.9%) generally precluded regression in isotope correlation diagrams. Plateau gas fractions were selected from age spectra using the criteria of Fleck et al. (1977), whereby a plateau consists of at least three successive incremental-heating steps, showing consistency within 2σ error and carrying $>50\%$ of the total ^{39}Ar gas released. The apparent ages calculated for each step are internally concordant; all age spectra are essentially flat and satisfy the plateau criteria. They yielded plateaux for 90.3–99.8% of the total released ^{39}Ar (Table 1), which is typical for thermally undisturbed volcanic sanidine (Duffield and Dalrymple, 1990). Discordant gas fractions are limited to initial increments showing high variance and low radiogenic argon yields. Weighted mean ages based on inverse variances were calculated for the plateaux, demonstrating that the main part of the Ptolemais Formation spans an interval from approximately 5.0 to 4.0 Ma (Table 1). The plateau ages are generally consistent with stratigraphic position. ^{40}Ar/^{39}Ar ages of the volcanic ash beds from the lower Kyrio member are systematically older than those from the middle Theodoxus member, while the volcanic ash beds from the upper Notio member have the youngest ages. Even within the three members, the ages are generally in agreement with the stratigraphic order. Noteworthy is that the biotite separate of sample SLM3T yielded an $\sim$120 kyr older plateau age than the sanidine separate of the same sample.

All nine sanidine separates were also analysed via single-step total fusion. The results are summarised in Table 1. From all but three sanidine separates, all

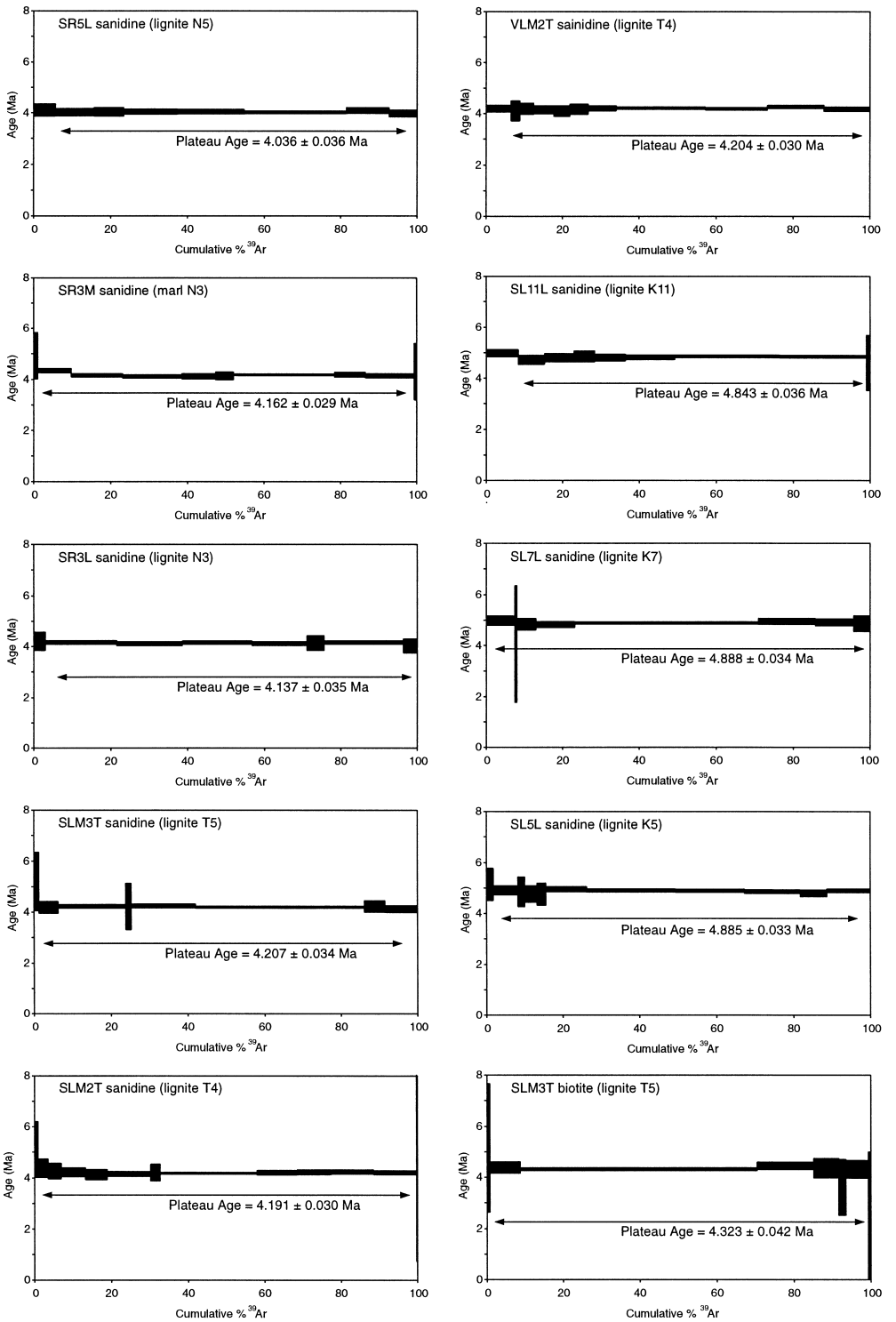

Fig. 4. $^{40}Ar/^{39}Ar$ laser incremental-heating spectra for sanidine and biotite separates from nine of the Ptolemais volcanic ash beds. Plateau definitions are as described by Fleck et al. (1977). For the location of the ash beds see Fig. 3. All errors shown are listed at the 2σ level, internal precision.

Table 1
All samples are from the Tomea Eksi section, except VLM2T which is from the Vorio section (see also Fig. 3)

Sample	Cycle	Material	APTS age (Ma)	$^{40}Ar/^{39}Ar$ age [a] (TCR = 27.92) (Ma)	K/Ca	^{39}Ar (%)	*n*1	MSWD	Δ (Ma)	Δ (%)	$^{40}Ar/^{39}Ar$ age [b] (TCR = 28.34) (Ma)	Δ (Ma)	Δ (%)	$^{40}Ar/^{39}Ar$ age [c] (TCR = 28.16) (Ma)	Δ (Ma)	Δ (%)
AGE SPECTRUM																
Irradiation VU16																
SR5L	N5	sanidine	4.280	4.036 ± 0.036	41.0	94.4	7	0.42	0.244	6.0	4.097	0.183	4.5	4.070	0.210	5.2
SR3M	N3	sanidine	4.308	4.162 ± 0.029	45.0	90.3	8	0.66	0.146	3.5	4.225	0.083	2.0	4.197	0.111	2.7
SR3L	N3	sanidine	4.324	4.137 ± 0.035	48.1	97.0	7	0.44	0.187	4.5	4.199	0.125	3.0	4.172	0.152	3.7
SLM3T	T5	sanidine	4.387	4.207 ± 0.034	97.9	98.8	7	0.45	0.180	4.3	4.270	0.116	2.7	4.243	0.144	3.4
SLM2T	T4	sanidine	4.408	4.191 ± 0.030	70.6	99.1	12	0.39	0.217	5.2	4.254	0.154	3.6	4.227	0.181	4.3
VLM2T	T4	sanidine	4.408	4.204 ± 0.030	62.1	93.5	10	0.79	0.204	4.9	4.267	0.141	3.3	4.240	0.168	4.0
SL11L	K11	sanidine	5.015	4.843 ± 0.035	39.0	91.6	8	0.54	0.172	3.6	4.916	0.099	2.0	4.884	0.131	2.7
SL7L	K7	sanidine	5.099	4.888 ± 0.034	35.2	99.8	8	0.59	0.211	4.3	4.962	0.137	2.8	4.929	0.170	3.5
SL5L	K5	sanidine	5.146	4.885 ± 0.033	20.6	98.2	10	0.73	0.261	5.3	4.958	0.188	3.8	4.926	0.220	4.5
Irradiation VU21																
SLM3T	T5	biotite	4.387	4.323 ± 0.042	21.8	98.6	7	0.93	0.063	1.5	4.388	−0.002	0.0	4.481	0.027	0.6

Sample	Cycle	Material	APTS age (Ma)	$^{40}Ar/^{39}Ar$ age [a] (TCR = 27.92) (Ma)	K/Ca	*n*2	MSWD	Δ (Ma)	Δ (%)	$^{40}Ar/^{39}Ar$ age [b] (TCR = 28.34) (Ma)	Δ (Ma)	Δ (%)	$^{40}Ar/^{39}Ar$ age [c] (TCR = 28.16) (Ma)	Δ (Ma)	Δ (%)
TOTAL FUSION															
Irradiation VU16															
SR5L	N5	sanidine	4.280	4.083 ± 0.023	37.5	5	1.32	0.197	4.8	4.144	0.136	3.3	4.118	0.162	4.0
SR3M	N3	sanidine	4.308	4.122 ± 0.026	35.5	5	2.35	0.186	4.5	4.184	0.124	3.0	4.157	0.151	3.7
SR3L	N3	sanidine	4.324	4.132 ± 0.026	45.0	5	0.63	0.192	4.6	4.194	0.130	3.1	4.167	0.157	3.8
SLM3T	T5	sanidine	4.387	4.158 ± 0.024	51.8	5	0.02	0.228	5.5	4.221	0.166	3.9	4.193	0.193	4.6
SLM2T	T4	sanidine	4.408	4.178 ± 0.023	53.3	5	2.02	0.230	5.5	4.241	0.167	3.9	4.213	0.195	4.7
VLM2T	T4	sanidine	4.408	4.224 ± 0.019	50.1	4	0.42	0.184	4.4	4.288	0.120	2.8	4.260	0.148	3.5
SL11L	K11	sanidine	5.015	4.888 ± 0.031	49.5	5	2.39	0.127	2.6	4.962	0.053	1.1	4.929	0.086	1.7
SL7L	K7	sanidine	5.099	4.862 ± 0.029	38.1	3	0.33	0.237	4.9	4.935	0.164	3.3	4.903	0.196	4.0
SL5L	K5	sanidine	5.146	4.841 ± 0.025	40.6	3	0.59	0.305	6.3	4.914	0.232	4.7	4.882	0.264	5.5
Irradiation VU21															
SLM2T	T4	sanidine	4.408	4.222 ± 0.023	50.9	12	1.19	0.186	4.4	4.286	0.122	2.9	4.258	0.150	3.6
SL7L	K7	sanidine	5.099	5.002 ± 0.051	36.1	12	16.38	0.097	1.9	5.077	0.022	0.4	5.044	0.055	1.1

Cycle number is from base of the Ptolemais Formation. APTS (astronomical) ages were obtained by linear interpolation of the sedimentation rate between astronomically dated calibration points, i.e. the lignite midpoints (see Van Vugt et al., 1998). $^{40}Ar/^{39}Ar$ ages [a] are quoted against TCR sanidine of 27.92 Ma (Wijbrans et al., 1995) and $^{40}Ar/^{39}Ar$ ages [b] against TCR sanidine of 28.34 Ma (Renne et al., 1998), both calculated with $\lambda = 5.543 \times 10^{-10}$ yr^{-1} and ^{40}K isotopic abundance of 0.01167% (Steiger and Jaeger, 1977). $^{40}Ar/^{39}Ar$ ages [c] are quoted against TCR of 28.16 Ma, calculated using the intercalibration coefficients between GA-1550, FCT and TCR of Renne et al. (1998), the branching coefficients of Endt (1990) and isotopic abundance of ^{40}K of 0.01167% (Garner et al., 1975). ^{39}Ar (%) is the percentage of total released ^{39}Ar used in the plateau age. *n*1 and *n*2 are the number of increments and single fusion experiments used for the plateau and total fusion ages, respectively. MSWD is the mean squared weighted deviation. Δ is the difference between the APTS and $^{40}Ar/^{39}Ar$ ages. Isotope interference corrections from measurements of CaF_2 and Fe-doped K-silicate glass were $(^{36}Ar/^{37}Ar)_{Ca} = 0.000264 \pm 0.0000017$; $(^{39}Ar/^{37}Ar)_{Ca} = 0.000673 \pm 0.0000037$; $(^{40}Ar/^{39}Ar)_{K} = 0.00086 \pm 0.00007$. Errors are reported at 2σ analytical precision. Copies of the full $^{40}Ar/^{39}Ar$ data set are available on request from the first author.

individual replicate analyses are concordant within the error limits of their weighted mean value. Their apparent $^{40}Ar/^{39}Ar$ ages are in excellent agreement with their stratigraphic order. For sanidine VLM2T, 4 out of 5 total fusion ages are indistinguishable at the 95% confidence level. The remaining run has a 60 kyr younger apparent age. Sanidine SL5L and SL7L gave less reliable $^{40}Ar/^{39}Ar$ dating results. Two individual runs of SL5L gave ~80 kyr older ages than the weighted mean value. Total fusion experiments on SL7L gave rather divergent results, with only three concordant analyses out of five after irradiation run VU16. Of the remaining two runs of SL7L one age was ~80 kyr older, while the other was ~540 kyr older. Analogous to the first experiment, individual analyses for SL7L after irradiation run VU21 showed considerable scatter around the mean with ages ranging between 4.989 and 5.119 Ma and a MSWD value of 16.38 (Table 1).

The volcanic ash bed from cycle T4 yielded two independent age estimates from samples collected at two localities, SLM2T and VLM2T. Both the single fusion and incremental-heating experiments gave $^{40}Ar/^{39}Ar$ ages, which were not statistically different at the 95% confidence level. For all samples, single fusion and incremental-heating experiments yielded ages that were indistinguishable (Table 1). Moreover, laser total fusion experiments on sanidine separate SLM2T yielded concordant weighted mean ages after irradiation runs VU16 and VU21 (Table 1). These experiments altogether have demonstrated the good reproducibility of the dating experiments.

5. Discussion and conclusions

5.1. Ptolemais composite section

All sections exposed in the Vorio, Tomea Eksi and Komanos open-pit mines contain both intervals in which rhythmic alternations of lignites and marls are very prominent, and intervals were indications for rhythmic sedimentation is less obvious or absent. The uniform presence of volcanic ash beds in these sections confirms the cyclostratigraphic correlations and indicates that the lignite–marl rhythmites represent regional, basin-wide sedimentary cycles rather than lateral facies migrations. Intervals without a clear expression of cyclicity often contain discontinuous fossiliferous levels or sand lenses, indicating a dominance of local (e.g. topography) over regional (e.g. climatically induced) control. To demonstrate that the lignite–marl cycles in the Ptolemais Basin are linked to orbital variations one must minimise these local effects. Any single section in the studied open-pit mines does not fulfil this purpose. In contrast to most deep-marine environments, local control generally plays an important role on facies development in shallow lacustrine deposits (Platt and Wright, 1992). Fortunately, the regular and consistent (i.e. laterally continuous) cyclic patterns for a particular stratigraphic interval are always present in at least one of the sections. The cyclostratigraphic Ptolemais composite section incorporates those intervals and thus shows an 'ideal' succession of lignite–marl cycles for the Ptolemais Basin.

Altogether, the Ptolemais composite section reveals 56 sedimentary cycles; 30 cycles in the Kyrio member (K1–K30), 6 cycles in the Theodoxus member (T1–T6) and 20 cycles in the Notio member (N1–N20). From the Tomea Eksi section, cycles K1–K12, K22–K30 and N1–N10 have been incorporated in the composite section. Cycles K13–K21 are taken from the Komanos section. All cycles from the Theodoxus member (T1–T6) and the upper 11 cycles from the Notio member (N11–N20) in the composite section are selected from the Vorio section (Fig. 5).

5.2. Precessional origin of lignite–marl cycles

The positions of the volcanic ash beds are well defined within the cyclostratigraphic composite section, and hence their $^{40}Ar/^{39}Ar$ ages provide the age-control necessary for calculating the average duration of a lignite–marl cycle. From each of the nine volcanic ash beds dated, we used both the plateau ages from the incremental-heating experiments and the weighted mean ages from the total fusion experiments. We plotted these versus the cumulative sedimentary cycle numbers from the base towards the top of the Ptolemais composite section (Fig. 6). The slope of a linear best-fit line through the data points equals the average duration of a lignite–marl cycle. A least-square linear regression using all 22 radiometric ages gives an average duration of 21.8 ± 0.8

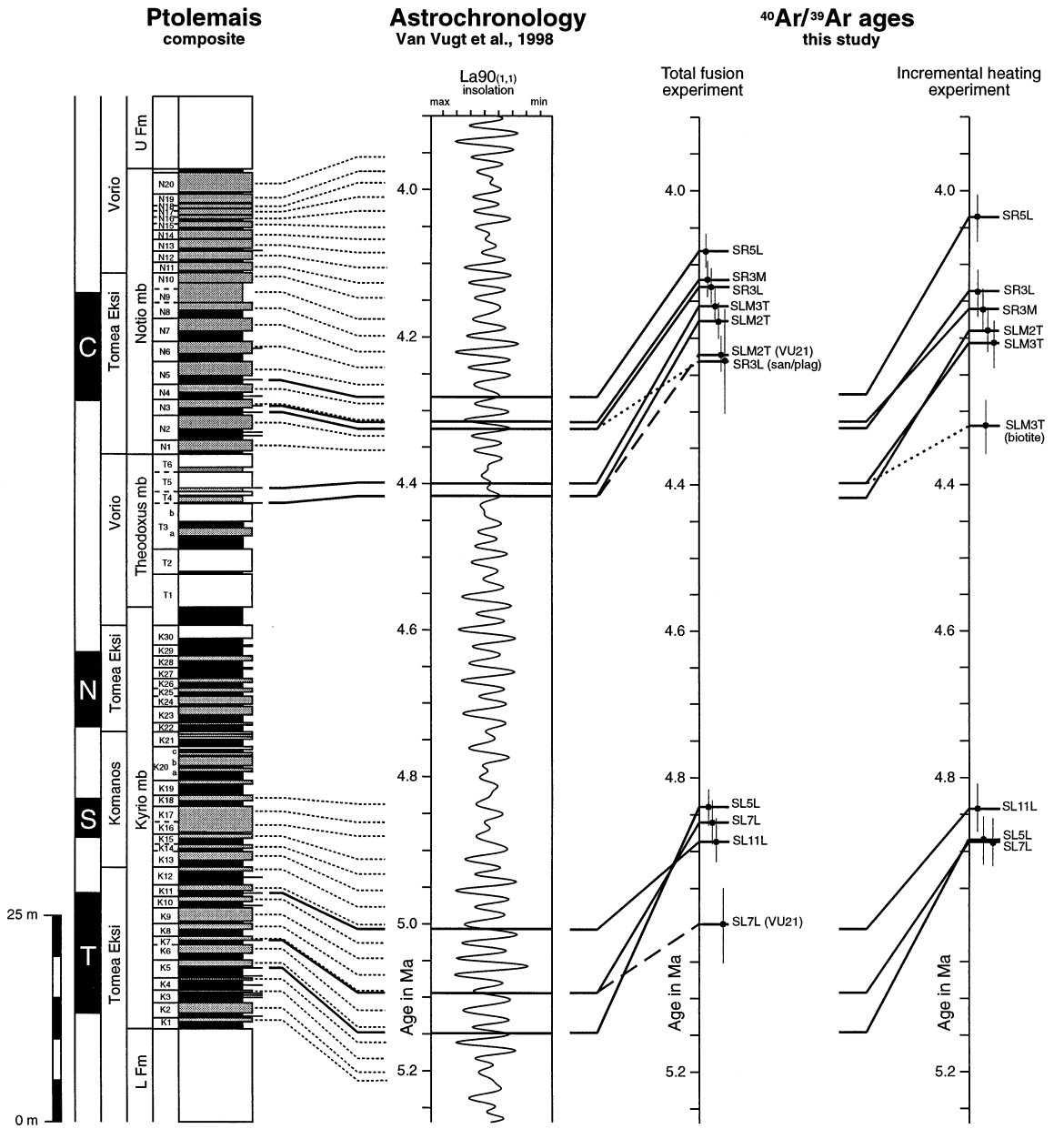

Fig. 5. Composite section showing the succession of lignite–marl cycles in the Ptolemais Formation. Magnetic polarity and partial sections are indicated to the left of the sedimentary cycle numbers and stratigraphic members. In the polarity column, black (white) indicates normal (reversed) polarity. *T*, *S*, *N* and *C* indicate the Thvera, Sidufjall, Nunivak and Cochiti Subchrons, respectively (for details see Van Vugt et al., 1998). Also shown is the comparison of incremental-heating and total fusion $^{40}Ar/^{39}Ar$ ages of nine volcanic ash beds with astronomical ages for the same beds. Astronomical ages were obtained by linear interpolation of the sedimentation rate between astronomically dated calibration points, i.e. the lignite midpoints (Van Vugt et al., 1998). Solid lines, which connect astronomical and $^{40}Ar/^{39}Ar$ ages, represent the VU16 sanidine separates. Dashed lines mark the VU21 sanidine separates, and dotted lines the VU21 biotite and VU10 mixed sanidine–plagioclase separates, respectively. All errors in the $^{40}Ar/^{39}Ar$ ages are at 2σ analytical precision.

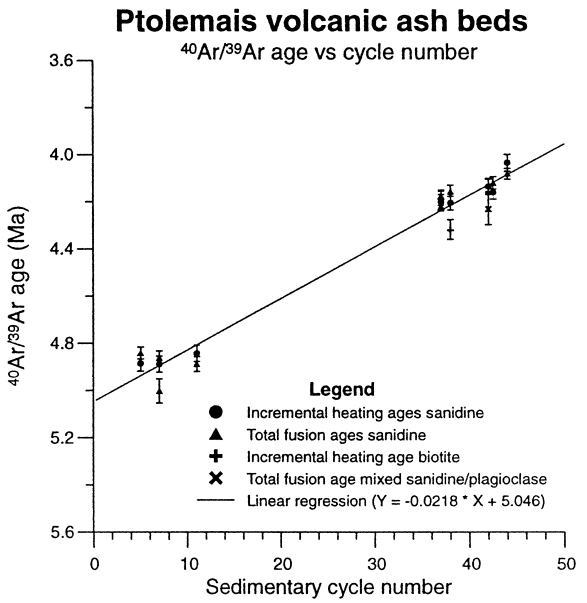

Fig. 6. Laser incremental-heating and total fusion $^{40}Ar/^{39}Ar$ ages of Ptolemais volcanic ash beds plotted vs. their corresponding cumulative sedimentary cycle number from the base of the Ptolemais Formation. Simple linear regression yields an average period of 21.8 ± 0.8 kyr for a lignite–marl cycle, which is in excellent agreement with the average periodicity of astronomical precession.

kyr for the deposition of a lignite–marl cycle. This duration is in excellent agreement with the 21.7 kyr average periodicity of astronomical precession. Evidently, the lignite–marl cycles in the Ptolemais Formation are linked to the precessional variation in the Earth's orbit through its influence on Mediterranean climate. To our knowledge, this is the first time that $^{40}Ar/^{39}Ar$ dating results — totally independent from any other dating and or tuning technique — confirm the astronomical theory of climate change.

Independently from our method, an astronomical control on the deposition of the sedimentary cycles has also been suggested by Van Vugt et al. (1998). They correlated the magnetic polarity sequence of the Ptolemais succession to the Astronomical Polarity Time Scale (APTS) and found an average duration of the lithological cycles of 21.6 ± 0.5 kyr.

5.3. Comparison of Ar/Ar and astronomical ages

The correlation of individual lignite–marl cycles to computed astronomical target curves by Van Vugt et al. (1998) resulted in astronomical ages for all sedimentary cycles, and thus for the intercalated volcanic ash layers. These astronomical ages have been obtained totally independent from our radioisotopic chronology. These two age estimates for the volcanic ash beds are compared in Table 1 and Fig. 5. It is striking that all $^{40}Ar/^{39}Ar$ ages are significantly younger than the corresponding astronomical ages. For the sanidine separates, the discrepancies between the two ages are close to 200 kyr (~4.5%). Such an age difference is beyond stated uncertainties, and so the astronomical ages must either be too old, or the $^{40}Ar/^{39}Ar$ ages too young (or both). Below, we will evaluate the possible sources of error in both age estimates.

The accuracy in the orbitally tuned chronology depends ultimately on (1) the correctness of the tuning, (2) the accuracy of the magnetostratigraphic data of the sedimentary succession studied, (3) accuracy of the orbital time-series used, and (4) errors in the APTS.

The orbitally tuned chronology used the magnetostratigraphy and biostratigraphy of the Ptolemais composite and the age of the corresponding reversal boundaries in the astronomically dated Rossello composite section (Langereis and Hilgen, 1991) for a first-order calibration; see Van Vugt et al., 1998. Sedimentary cycles in the Rossello section were calibrated to the summer insolation time series by Lourens et al. (1996), thus providing astronomical ages for the magnetic reversal boundaries as well. The thus obtained astronomical ages for the magnetic reversal boundaries served as approximate tie-points for the astronomical tuning of the sedimentary cycles in the Ptolemais composite. Subsequent tuning to insolation resulted in astronomical ages for all the sedimentary cycles in the Ptolemais succession. The tuning shows a good-fit between insolation and typical sedimentary cycle patterns, like the well developed cycles in the Notio member or the absence of an apparent cyclicity in the Theodoxus member. Furthermore, the positions of the reversal boundaries generally appear within the same lithological cycle as in the APTS/Rossello composite (Van Vugt et al., 1998). Consequently, we consider the orbital-tuned chronology to be accurate within one precession cycle, that is less than 21 kyr, and believe that the discrepancy unlikely originated from incorrectness in the orbital tuning.

The alternative is that the magnetostratigraphy of the Ptolemais succession is subject to error. The Ptolemais magnetostratigraphy reveals a dominantly reversed polarity with four normal intervals (Fig. 5). Given its Early Pliocene age (Van de Weerd, 1979), these normal intervals have been correlated to the four normal Subchrons of the Gilbert Chron; see Van Vugt et al. (1998) for details. A possible source of error might be delayed acquisition of the magnetic remanence. However, delayed acquisition of the magnetisation in the Ptolemais sequence cannot explain the discrepancy between $^{40}Ar/^{39}Ar$ and astronomical ages. This would result in older astronomical ages for the volcanic ash beds rather than younger ages. Again, support for the correctness of the magnetostratigraphy comes from the fact that the positions of the reversal horizons generally appear within the same lithological cycle as in the APTS/Rossello composite (Van Vugt et al., 1998). Thus, errors in the Ptolemais magnetostratigraphy cannot explain the age discrepancy.

Inaccuracy of the orbital time series will not result in a 200-kyr difference between the astronomical and radioisotopic ages at 4 or 5 Ma. Continuing improvements of the astronomical calculations resulted in a solution that is very accurate for at least the last 3 million years (Quinn et al., 1991). Because of its complexity, the error in the astronomical solution is difficult to estimate. It is believed to be less than $\sim$0.03 radians for the Earth's longitude and pole position at 3.0 Ma, which is of the order of only a few hundred years. Thus, inaccuracy in the orbital solutions can at most generate a negligible error in the astronomical age estimates.

As explained above, Van Vugt et al. (1998) use the astronomical ages of the magnetic reversal boundaries in the Rossello section — on which the APTS is based — as approximate tie-points for the orbital tuning of the sedimentary cycles in Ptolemais. These astronomical ages were derived from correlation of a detailed record of carbonate cycles to astronomical time series (Hilgen, 1991; Lourens et al., 1996). Therefore, the discrepancy might be explained by too old astronomical ages for the reversal boundaries in the Rossello section. This might result from delayed acquisition of magnetisation or by an incorrect correlation of the sedimentary cycles to the astronomical time series. Both options seem unlikely. Detailed magnetostratigraphic studies of the Rossello section (Van Hoof and Langereis, 1991; Langereis and Hilgen, 1991) limit the influence of delayed acquisition to less than two sedimentary cycles, that is less than 42 kyr. Independent support for the correlation of the carbonate cycles to the astronomical time series came from GRAPE density (Shackleton et al., 1990, 1995) and dust flux (Tiedemann et al., 1994) oscillations in deep-sea records. Further confirmation for the APTS came from a study by Wilson (1993), who showed that the astrochronology resulted in a more consistent and steady history of sea floor spreading rates. Consequently, a systematic error in the age of the reversal boundaries in the Rossello composite section seems unlikely.

Thus, it is tentatively concluded that the discrepancy between the astronomical and isotopic ages for the Ptolemais volcanic ash beds cannot be explained by systematically too old astronomical ages. In addition to errors in the orbitally tuned chronology, the other option might be that the $^{40}Ar/^{39}Ar$ age estimates are systematically too young. Too young isotopic ages may result from (1) partial loss of radiogenic ^{40}Ar, (2) an underestimation of the contribution of Ca- and K-derived Ar isotopes, (3) uncertainties in the age of the neutron-fluence monitor or primary standards, and/or (4) errors in the values of the decay constants of ^{40}K.

Neither loss of radiogenic ^{40}Ar, nor an underestimation of the contribution of Ca- and K-derived Ar isotopes are likely causes for the discrepancy. Incremental-heating experiments allow for evaluation of the possible influence of radiogenic argon loss. The generally uniform distribution of the $^{40}Ar/^{39}Ar$ ratios (Fig. 4) suggests a closed system with no influence of post-depositional alteration or thermal disturbances (Hess and Lippolt, 1986). The low coalification stage of the lignites (Cameron et al., 1984; Kaouras, 1989) also argues against possible thermal disturbances. The contribution of neutron produced Ar isotopes from Ca and K is not a significant source of error in this study either, as indicated by the uniformly high K/Ca ratios of the dated separates (Table 1).

In addition, too young $^{40}Ar/^{39}Ar$ ages may result from errors in the ages of the (primary and secondary) standards. $^{40}Ar/^{39}Ar$ dating is a relative dating method, i.e. $^{40}Ar/^{39}Ar$ ages are quoted rela-

tive to primary standards whose ages are determined by the $^{40}K/^{40}Ar$ method, or on secondary standards whose ages are based on $^{40}Ar/^{39}Ar$ intercalibration with primary standards. Recent intercalibrations of several internationally used standards have eliminated intercalibration of standards as a significant source of error in $^{40}Ar/^{39}Ar$ dating (Baksi et al., 1996; Renne et al., 1998). Until now, however, the absolute ages of $^{40}Ar/^{39}Ar$ monitor standards remain an unresolved issue. In our age calibration we have used an age for the monitor standard TCR sanidine of 27.92 Ma, quoted relative to a K–Ar age of 162.9 Ma of the primary standard SB-3 biotite (Lanphere et al., 1990). Baksi et al. (1996) reported an age for TCR sanidine of 28.0 Ma, cited relative to a similar age for SB-3 biotite. Renne et al. (1998) obtained a total fusion age of 28.34 Ma for TCR, based on 54 isotopic measurements. Their age for TCR is quoted relative to a $^{40}Ar/^{40}K$ age of 98.79 ± 0.96 Ma for the primary standard GA-1550. It should be noted that this age is somewhat older but statistically indistinguishable from the age of 97.9 ± 0.9 Ma calculated from the original data of McDougall and Roksandic (1974). Using the equation of Dalrymple et al. (1993), we have recalculated our $^{40}Ar/^{39}Ar$ ages with an age of 28.34 ± 0.28 Ma for TCR as suggested by Renne et al. (1998). This reduces the 4.5% age discrepancy by ~1.5% (Table 1), to a still significant ~3% discrepancy.

Inaccuracies in the values of the decay constants might also be a source of error for our $^{40}Ar/^{39}Ar$ ages. Beckinsale and Gale (1969) summarised the available determinations of the specific activities for the various decay modes of ^{40}K. These data were combined with a new atomic abundance for ^{40}K (Garner et al., 1975) to calculate the decay constants recommended by Steiger and Jaeger (1977). These calculations gave a total decay constant λ of ^{40}K of $(5.543 \pm 0.010) \times 10^{-10}$ yr^{-1}, and a half-life of $(1.250 \pm 0.002) \times 10^9$ yr. We have used these values in our age calculations. It is noteworthy that these values are at odds with values used since 1973 by the nuclear physics and chemistry communities. Endt (1990) cites a half-life of $(1.277 \pm 0.008) \times 10^9$ yr for ^{40}K, based on branching coefficients of 89.33% for β^- decay and 10.67% for electron capture decay, and a value of $(1.178 \pm 0.004) \times 10^{-2}$% for the ^{40}K abundance. The value for the isotopic ^{40}K abundance was based on measurements done by Nier (1950) and Reuterswärd (1956). It deviates significantly from the generally accepted isotopic abundance value for ^{40}K of $(1.167 \pm 0.0004) \times 10^{-2}$% as determined by Garner et al. (1975). The latter value, which was calculated from standards of known composition, prepared by gravimetrically mixing, is probably more accurate than the ones by Nier (1950) and Reuterswärd (1956), who used older, less accurate techniques. Therefore, we have used the value of Garner et al. (1975) in our work. We have recalculated the age of GA-1550 of Renne et al. (1998), using only the branching coefficients of Endt (1990) and neglecting the isotopic abundance value for ^{40}K as reported in Endt (1990). Instead we take the isotopic abundance for ^{40}K of Garner et al. (1975), the ^{40}K concentration of Renne et al. (1998) and the $^{40}Ar^*$ measurements of McDougall and Roksandic (1974). The age of GA-1550 is recalculated to 98.23 Ma. With this value for GA1550 and the intercalibration factors for GA1550, FCT and TCR of Renne et al. (1998) the age of TCR is recalculated to 28.16 Ma. We have again recalculated our own $^{40}Ar/^{39}Ar$ ages with this value for TCR (Table 1). This resulted in a reduction of the age discrepancy of ~1% compared to the original values (Table 1), but still leaving an ~3.5% (140–175 kyr) discrepancy.

The mineral sanidine is generally believed to be the ideal mineral for $^{40}Ar/^{39}Ar$ dating, because of its high K_2O content and resistance against weathering (McDougall and Harrison, 1988). Therefore, we have focused on the sanidine populations in the $^{40}Ar/^{39}Ar$ experiments. In general, the biotite crystals in the Ptolemais ashes have been (partially) altered to chlorite, and are, consequently, less suitable for dating. The only exception is the ash in cycle T5 in the Theodoxus member, which contains fresh and unaltered biotite crystals. For comparison, we have also dated a biotite separate of this ash (sample SLM3T), which yielded a ~120 kyr older plateau age than the sanidine separate of the same sample (Table 1; Fig. 5). Therefore, the biotite separate SLM3T resulted in an (uncorrected) $^{40}Ar/^{39}Ar$ age that is in closer agreement with the astronomical age than the experiment on pure sanidine separates. However, given the fact that from one ash only biotite and sanidine minerals have both been dated, and considering the uncertainties in the corrections

discussed above, no far reaching consequences can be drawn from this inconsistency. Moreover, the literature is replete with examples to the contrary (e.g. Spell and McDougall, 1992; Turrin et al., 1994; Izett and Obradovich, 1994; Smith et al., 1996; Hilgen et al., 1997).

In conclusion, the ~200 kyr age discrepancy between the astronomical and $^{40}Ar/^{39}Ar$ ages of the volcanic ash beds in the Ptolemais composite remains difficult to explain. The discrepancy is beyond the errors in both the astronomical and the $^{40}Ar/^{39}Ar$ ages. Possible sources of error in the astronomical ages include incorrectness of the tuning, inaccuracies of the magnetostratigraphic data or the orbital time-series used, and/or errors in the Rossello section, on which the APTS is based. However, none of these seems to have significantly contributed to the ~200 kyr discrepancy. The other option is that the $^{40}Ar/^{39}Ar$ age estimates are systematically too young. From the excellent $^{40}Ar/^{39}Ar$ data set it is evident that neither loss of radiogenic ^{40}Ar, nor an underestimation of the contribution of Ca- and K-derived Ar isotopes are significant sources of error. Moreover, only part of the discrepancy might result from the use of erroneously young ages for the neutron-fluence monitors, and/or incorrect values for the decay constants of ^{40}K. Clearly, as noted by Renne et al. (1998), improved determination of decay constants and absolute ages of monitor standards are necessary to increase the accuracy of the $^{40}Ar/^{39}Ar$ method. Our ongoing research aims at a more robust intercalibration of $^{40}Ar/^{39}Ar$ and astronomical time using astronomically dated volcanic ash beds in both marine and continental successions.

Acknowledgements

Prof. Dr. C.S. Doukas and Prof. Dr. E. Velitzelos (University of Athens, Greece) are greatly acknowledged for arranging necessary contacts and for co-operation in the field. We are grateful to the Public Power Corporation (Δ.Ε.Η./Λ.Κ.Π.-Α.) for permission to work in the mines and to the corporation's employees for their hospitality and assistance in the field. The authors thank Hendrik-Jan Bosch, Mark Dekkers, Marloes van Hoeve, Cor Langereis, Rob Satter, Konstantin Theocharopoulos and Wout Krijgsman for their interesting discussions and assistance in the field. We thank the reviewers T.C. Johnson and P.R. Renne for their valuable comments on an earlier version of the manuscript. This work was partly supported by the Netherlands Geosciences Foundation (GOA) with financial aid from the Netherlands Organisation for Scientific Research (NWO grant to J.S. and N.V.V.). This is NSG publication 990105.

References

Anastopoulos, J., Koukouzas, C.N., 1972. Economic geology of the southern part of the Ptolemais lignite basin (Macedonia, Greece). Geol. Geophys. Res. 16 (1), 1–189.

Anderson, R.Y., 1982. A long geoclimatic record from the Permian. J. Geophys. Res. 87 (C9), 7285–7294.

Baksi, A.K., Archibald, D.A., Farrar, E., 1996. Intercalibration of $^{40}Ar/^{39}Ar$ dating standards. Chem. Geol. 129, 307–324.

Barrell, J., 1917. Rhythms and the measurements of geologic time. GSA Bull. 28, 745–904.

Bates, R.L., Jackson, J.A.E., 1987. Glossary of Geology. American Geological Institute, Alexandria, VA.

Beckinsale, R.D., Gale, N.H., 1969. A reappraisal of the decay constants and branching ratio of ^{40}K. Earth Planet. Sci. Lett. 6, 289–294.

Bradley, W.H., 1929. The varves and climate of the Green River epoch. U.S. Geol. Surv. Prof. Pap. 158E, 87–110.

Brunn, J.H., 1956. Étude geologique du pinde serpetional et de la Macedoine occidentale. Ann. Géol. Pays Hellen. 7, 1–358.

Cameron, A.R., Kalkreuth, W.D., Koukouzas, C., 1984. The petrology of Greek brown coals. Int. J. Coal Geol. 4, 173–207.

Dalrymple, G.B., Duffield, W.A., 1988. High precision $^{40}Ar/^{39}Ar$ dating of Oligocene rhyolites from the Mogollon–Datil volcanic field using a continuous laser system. Geophys. Res. Lett. 15 (5), 463–466.

Dalrymple, G.B., Izett, G.A., Snee, W., Obradovich, J.D., 1993. $^{40}Ar/^{39}Ar$ age spectra and total-fusion ages of tektites from Cretaceous–Tertiary boundary sedimentary rocks in the Beloc Formation, Haiti. U.S. Geol. Surv. Bull. 2065, 1–20.

Dean, W.E., Fouch, T.D., 1983. Lacustrine environments. In: Scholle, P.A., Bebout, D., Moore, D. (Eds.), Carbonate Depositional Environments. Am. Assoc. Pet. Geol. Mem. 33, 97–130.

Duffield, W.A., Dalrymple, G.B., 1990. The Taylor Creek Rhyolite of New Mexico: a rapidly emplaced field of lava domes and flows. Bull. Volcanol. 52, 475–478.

Ehlers, E., 1960. Bericht über die bisher im Rahmen der Expertise Ptolemais durchgeführten geologischen und paläontologischen Untersuchungen. Bundesanstalt für Geowissenschaften und Röhstoffen, Hannover, pp. 1–36.

Emiliani, C., 1955. Pleistocene temperatures. J. Geol. 63, 538–578.

Endt, P.M., 1990. Energy levels of A = 21–44 nucleii. Nucl. Phys. A521, 1–830.

Fischer, A.F., 1980. Gilbert – bedding rhythms and geochronology. GSA Spec. Pap. 183, 93–104.

Fleck, R.J., Sutter, J.F., Elliot, D.H., 1977. Interpretation of discordant $^{40}Ar/^{39}Ar$ age-spectra of Mesozoic tholeiites from Antarctica. Geochim. Cosmochim. Acta 41, 15–32.

Garner, E.L., Murphy, T.J., Gramlich, J.W., Paulsen, P.J., Barnes, I.L., 1975. Absolute isotopic abundance ratios and the atomic weight of a reference sample of potassium. J. Res. Natl. Bur. Stand. 79A, 713–725.

Gilbert, G.K., 1895. Sedimentary measurement of geological time. J. Geol. 3, 121–127.

Gramann, A., 1960. Die Fossilien des Braunkohlenbeckens von Ptolemais, Komanos. Bundesanstalt für Geowissenschaften und Röhstoffen, Hannover, pp. 37–49.

Gregor, H.J., Velitzelos, E., 1995. Facies development of Greek browncoals – dependent on tectonic movements. Ann. Géol. Pays Hellen. 36, 731–739.

Hays, J.D., Imbrie, J., Shackleton, N.J., 1976. Variations in the Earth's orbit: pacemaker of the ice ages. Science 194, 1121–1132.

Hess, J.C., Lippolt, H.J., 1986. $^{40}Ar/^{39}Ar$ ages of tonstein and tuff sanidines: new calibration points for the improvement of the Upper Carboniferous time scale. Chem. Geol. (Isot. Geosci. Sect.) 59, 143–154.

Hilgen, F.J., 1991. Extension of the astronomically calibrated (polarity) time scale to the Miocene/Pliocene boundary. Earth Planet. Sci. Lett. 107, 349–368.

Hilgen, F.J., Krijgsman, W., Langereis, C.G., Lourens, L.J., Santarelli, A., Zachariasse, W.J., 1995. Extending the astronomical (polarity) time scale into the Miocene. Earth Planet. Sci. Lett. 136, 495–510.

Hilgen, F.J., Krijgsman, W., Wijbrans, J., 1997. Direct comparison of astronomical and $^{40}Ar/^{39}Ar$ ages of ash beds: potential implications for the age of mineral standards. Geophys. Res. Lett. 24 (16), 2043–2046.

Imbrie, J., Hays, J.D., Martinson, D.G., McIntyre, A., Mix, A.C., 1984. The orbital theory of Pleistocene climate: support from a revised chronology of the marine $\delta^{18}O$ record. In: Berger, A., Imbrie, J., Hays, J., Kukla, G., Saltzman, B. (Eds.), Milankovitch and Climate 1, Reidel, Dordrecht, p. 510.

Izett, G., Obradovich, J., 1994. $^{40}Ar/^{39}Ar$ age constraints for the Jaramillo normal subchron and the Matuyama–Brunhes geomagnetic boundary. J. Geophys. Res. 99, 2925–2934.

Kaouras, G., 1989. Kohlenpetrographische, Palynologische und Sedimentologische Untersuchungen der Pliozänen Braunkohle von Kariochori bei Ptolemais/NW Griechenland. Mathematisch-Naturwissenschaftlichen Fachbereiche, Ph.D. Thesis, Georg-August-Universität, Göttingen.

Kolios, N., Innocenti, F., Manetti, P., Peccerillo, A., Giliani, O., 1980. The Pliocene Volcanism of the Voras Mts (Central Macedonia, Greece). Bull. Volcanol. 43 (3), 553–568.

Koufos, G.D., Pavlides, S.B., 1988. Correlation between the continental deposits of the lower Axios Valley and the Ptolemais Basin. Bull. Geol. Soc. Gr. 20 (2), 9–19.

Krijgsman, W., Hilgen, F.J., Langereis, C.G., Santarelli, A., Zachariasse, W.J., 1995. Late Miocene magnetostratigraphy, biostratigraphy and cyclostratigraphy in the Mediterranean. Earth Planet. Sci. Lett. 136, 475–494.

Langereis, C.G., Hilgen, F.J., 1991. The Rossello composite: a Mediterranean and global reference section for the Early to early Late Pliocene. Earth Planet. Sci. Lett. 104, 211–225.

Lanphere, M.A., Dalrymple, G.B., Fleck, R.J., Pringle, M.S., 1990. Intercalibration of mineral standards for K–Ar and $^{40}Ar/^{39}Ar$ measurements. EOS, Trans. Am. Geophys. Union 71, 1658.

Lourens, L.J., Antonarakou, A., Hilgen, F.J., Van Hoof, A.A.M., Vergnaud-Grazzini, C., Zachariasse, W.J., 1996. Evaluation of the Plio-Pleistocene astronomical timescale. Paleoceanography 11 (4), 391–413.

McDougall, I., Harrison, T.M., 1988. Geochronology and thermochronology by the $^{40}Ar/^{39}Ar$ method. Oxford Monographs on Geology and Geophysics, 9, Oxford University Press, New York, 212 pp.

McDougall, I., Roksandic, Z., 1974. Total fusion $^{40}Ar/^{39}Ar$ ages using HIFAR reactor. J. Geol. Soc. Aust. 21, 81–89.

Mercier, J.L., Sorel, D., Vergely, P., 1989. Extensional tectonic regimes in the Aegean basins during the Cenozoic. Basin Res. 2, 49–71.

Murphy, D.H., Wilkinson, B.H., 1980. Carbonate deposition and facies distribution in a central Michigan marl lake. Sedimentology 27, 123–135.

Nier, A.O., 1950. A redetermination of the relative abundances of the isotopes of carbon, nitrogen, oxygen, argon, and potassium. Phys. Rev. 77, 789–793.

Papakonstantinou, A., 1979. Die hydrogeologischen Verhältnisse im Raum der Ptolemais-Senke und des westlichen Vermiongebirges in Griechisch-Mazedonien. Berliner Geowiss. Abh. 13, 1–79.

Pavlides, S.B., Mountrakis, D.M., 1986. Neotectonics of the Florina–Vegoritis–Ptolemais Neogene Basin (NW Greece): an example of extensional tectonics of the greater Aegean area. Ann. Géol. Pays Hellen. 33 (1), 311–327.

Platt, N.H., Wright, V.P., 1992. Palustrine carbonates and the Florida Everglades: towards an exposure index for the freshwater environment. J. Sediment. Petrol. 62 (6), 1058–1071.

Quinn, T.R., Tremaine, S., Duncan, M., 1991. A three million year integration of the Earth's orbit. Astron. J. 101, 2287–2305.

Renne, P.R., Swisher, C.C., Deino, A.L., Karner, D.B., Owens, T.L., DePaolo, D.J., 1998. Intercalibration of standards, absolute ages and uncertainties in $^{40}Ar/^{39}Ar$ dating. Chem. Geol. 145, 117–152.

Reuterswärd, C., 1956. On the isotopic constitution of potassium: a study of mass discrimination in a hot anode ion source. Ark. Fys. 11, 1–54.

Shackleton, N.J., Opdyke, N.D., 1973. Oxygen isotope and paleomagnetic stratigraphy of Pacific core V28-238: oxygen and isotope temperatures and ice volumes on a 10^5 and 10^6 year scale. Quat. Res. 3, 39–55.

Shackleton, N.J., Berger, A., Peltier, W.R., 1990. An alternative astronomical calibration of the lower Pleistocene timescale

based on ODP site 677. Trans. R. Soc. Edinburgh, Earth Sci. 81, 251–261.

Shackleton, N.J., Crowhurst, S., Hagelberg, T., Pisias, N.G., Schneider, D.A., 1995. A new Late Neogene time scale: application to leg 138 sites. Proc. ODP, Sci. Results 138, 73–97.

Smith, P.E., York, D., Chen, Y., Evensen, N.M., 1996. Single crystal ^{40}Ar–^{39}Ar dating of a Late Quaternary paroxysm on Kos, Greece: concordance of terrestrial and marine ages. Geophys. Res. Lett. 23 (21), 3047–3050.

Spell, T.L., McDougall, I., 1992. Revisions of the age of the Brunhes–Matuyama boundary and the Pleistocene Geomagnetic Polarity Timescale. J. Geophys. Res. 19, 1181–1184.

Steiger, R., Jaeger, E., 1977. Subcommission on geochronology: convention on the use of decay constants in geo- and cosmochronology. Earth Planet. Sci. Lett. 36, 359–362.

Tiedemann, R., Sarnthein, M., Shackleton, N.J., 1994. Astronomical timescale for the Pliocene Atlantic $\delta^{18}O$ and dust flux records of the Ocean Drilling Program site 659. Paleoceanography 9 (4), 619–638.

Turrin, B.D., Donnelly-Nolan, J.M., Hearn, B.C.J., 1994. $^{40}Ar/^{39}Ar$ ages from the rhyolite of Alder Creek, California: age of the Cobb Mountain normal-polarity subchron revisited. Geology 22, 251–254.

Van de Weerd, A., 1979. Early Ruscinian rodents and lagomorphs (Mammalia) from the lignites near Ptolemais (Macedonia, Greece). Proc. Kon. Akad. Wetensch. Amsterdam B82 (2), 127–170.

Van de Weerd, A., 1983. Palynology of some Upper Miocene and Pliocene Formations in Greece. Geol. Jahrb. B 48, 3–63.

Van Hoof, A.A.M., Langereis, C.G., 1991. Reversal records in marine marls and delayed acquisition of remanent magnetization. Nature 351, 223–225.

Van Houten, F.B., 1964. Cyclic lacustrine sedimentation, Upper Triassic Lockatong Formation, Central New Jersey and adjacent Pennsylvania. Kansas Geol. Surv. Bull. 169, 497–531.

Van Vugt, N., Steenbrink, J., Langereis, C.G., Hilgen, F.J., Meulenkamp, J.E., 1998. Magnetostratigraphy-based astronomical tuning of the early Pliocene lacustrine sediments of Ptolemais (NW Greece) and bed-to-bed correlation with the marine record. Earth Planet. Sci. Lett. 164, 535–551.

Velitzelos, E., Schneider, H., 1973. Beitrage zur Geologie West-Makedoniens 1. Elephantiden-Reste aus dem Pleistozän der Provinz Florina. Ann. Mus. Goulandris 1, 251–256.

Vetoulis, D.G., 1957. Beitrage zur Kenntnis der Geologie des Ptolemais-Beckens, Mazedoniens. Ann. Géol. Pays Hellen. 8, 48–79.

Wijbrans, J.R., Pringle, M.S., Koppers, A.A.P., Scheveers, R., 1995. Argon geochronology of small samples using the Vulkaan argon laserprobe. Proc. Kon. Akad. Wetensch. Amsterdam 98 (2), 185–218.

Wilson, D.S., 1993. Confirmation of the astronomical calibration of the magnetic polarity time scale from sea-floor spreading rates. Nature 364, 788–790.